This article was published in Journal of Nuclear Materials.
Journal homepage: www.elsevier.com/locate/jnucmat
Journal of Nuclear Materials 440 (2013) 158–168
DOI: http://dx.doi.org/10.1016/j.jnucmat.2013.04.059

Influence of impurity-vacancy disorder on characteristics of gadolinium-doped ceria oxide: Molecular dynamics study.

M.A. Kovalenko[a], A.Ya. Kupryazhkin[a]
[a] Ural Federal University, 620002, Mira street 19, Yekaterinburg, Russia
akm_max@mail.ru kupr@dpt.ustu.ru
Corresponding author: M.A. Kovalenko, akm_max@mail.ru +7(902)8729297,
623704, Berezovsky city, Betonshikov street 9

Abstract

By high-speed MD method using GPU the CGO nanocrystals of about 40,000 particles during about 0.1μs, in the temperature range (2500-700)K, were simulated. The influence of different dopant distributions on the nanocrystal characteristics, for two potentials sets, was investigated. For a given potentials set Gd distribution does not affect the lattice parameter and the anion diffusion coefficients. Five types of impurity vacancies were defined, by the Gd number in the nearest neighborhood, and temperature dependences were built. The formation energies of vacancies of all types were obtained.

Calculated by the MD conductivity activation energy of 0.6eV acceptable coincides with the experimental 0.7eV, just as the absolute conductivity values. The supposition that helium in CGO ceramics dissolve in vacancies, surrounded only by cerium ions, was discussed. Analysis of the MD, conductivity measurements and helium defectoscopy shows that up to the melting temperature the vacancies are mainly associated with impurity ions.

Keywords: molecular dynamics, cerium oxide, nanocrystal, dopant distribution, helium dissolution, vacancy association.

1. Introduction

Gadolinium-doped ceria ceramics is an excellent surrogate material to oxide nuclear fuel investigation as ceria is a structural analogue of uranium dioxide with similar thermophysical properties, and gadolinium is used as burnable poison in oxide nuclear fuel. Additional interests show the investigations of retention and release of alpha-decay products in the oxide nuclear fuel with gadolinium, and the mass transfer characteristics in the $Ce_{1-X}Gd_XO_{2-X/2}$ (CGO) system used in solid oxide fuel cells.

Molecular dynamics (MD) is widely used and very popular method for studying the structure and transport properties of CGO system. In this system, the cation mobility is very low even at temperatures slightly below the melting point and it can be assumed that there are no diffusion hops of the cations during MD calculations. Thus, the cations are almost motionless, except for thermal vibrations.

In most studies (e.g. [1-3]) the authors randomly distribute isolated Gd ions. We know only the one paper [4] in which the authors randomly distributed isolated Gd ions and Gd-Gd ion pairs, and compared the lattice parameter (LP) for the resulting distributions between itself and the experimental data. According to Inaba [4], the Gd distribution (GdD) influence essentially on the LP which was calculated for different X at room temperature, and the difference in the LP values for the isolated and pair GdD increased with X increasing. Unfortunately no author introduce any quantitative criteria of GdD obtained during simulation, and at the same time it is clear that for a large quantity of impurity ions with their random initial distribution the different Gd complexes of arbitrary size can be formed.

GdD can have a great influence on the fabrication technology of the CGO ceramics. With the decreasing temperature the dopant cations with other valences

tend to be associated, i.e. to the form a pairs or complexes. Different quenching rate of the ceramics can lead to a different GdD, which at low temperatures can remain unchanged (and non-equilibrium) or relax for a long time - months and years, which in turn may influence its technological parameters.

Impurity distribution can be extremely important and in the MD simulations, due to its possible influence on calculated macro parameters: on the one hand, due to the low mobility of cations equilibrium distribution of impurities in the MD at temperatures below the melting point is unattainable; on the other hand, the quality of the MD calculations is determined by the quantitative reproducibility of experimental macro parameters. Moreover, many sets of pair interaction potentials are obtained by fitting to the experimental data. It is interesting to introduce the quantitative estimation of GdD and to investigate in details the GdD influence on the resulting lattice parameter, anion diffusion coefficient, as well as to study the mechanisms of helium atoms dissolution in the CGO oxide ceramics to simulate the accumulation of alpha-decay products in the oxide nuclear fuel with burnable poison.

In brief, the in this work we try to:

1) Introduce some quantitative estimation of GdD in the impurity system.
2) Evaluate the GdD influence on the macroscopic quantities (the lattice parameter and the anion diffusion coefficient).
3) Investigate the anion vacancy distribution on the microscopic level, for various GdD.
4) Suggest and justify the mechanism of helium atoms dissolution in impurity anion vacancies and compare it with experiment data.

2. Simulation method

2.1. MD details

In this paper we have used the self-made program for ionic crystals simulation by classical molecular dynamics (MD) method, with the calculation of

interparticle forces on the graphics processor unit (GPU), using the interaction pair potentials in the approximation of rigid ions. MD method, the GPU performance and used in the present study interaction potentials were described in detail in our previous work [5]. The calculations were performed on the Radeon5870 and Radeon6970 graphics cards. The base code for calculating of the forces on the GPU was taken at [6] and further developed for the calculation of any number of particles types in the simulated system.

Simulations were carried out under isolated boundary conditions - a crystal of finite size with the octahedron form in a vacuum. We used empirical potentials in the approximation of rigid ions with non-formal charges. According to comparison of various potentials in the rigid ion approximation and in the shell model approximation for UO_2 system in [7-9], using in the current work empirical potentials give the best reproducibility of experimental data.

Gd ions in the system $Ce_{1-X}Gd_XO_{2-X/2}$ were distributed by different methods on the pure CeO_2 relaxed octahedron, using particles coordinates averaged by 1000 MD steps at a temperature of 100K. Impurity concentration for all simulations was equal to X=0.2, so we worked with the $Ce_{0.8}Gd_{0.2}O_{1.9}$ system. For each obtained GdD a series of simulations was carried out down from melting point with temperature step of 50K. The simulated system with previously obtained [5] pair potentials (referred to KMKA12) was consisted of 39,150 particles, which allowed us to obtain a good statistics to determine the anion diffusion coefficients and to eliminate the influence of the surface on the interior region of the nanocrystal.

For simulations with Inaba potentials the system consisted of 11,600 particles in order to save the computational resources. As shown in [5], the diffusion coefficients for the system of 8,000 ions do not differ from 40,000 ions, and the main purpose was to compare the simulation results with each other for different GdD for the same set of pair potentials.

Inaba potentials set was chosen for comparison for two reasons. First, it was the only one developed in the rigid ion approximation among available potentials when we began this investigation. And second, although the Inaba potentials

demonstrate greater melting temperature than the experimental one [5] other potentials in the rigid ion approximation show even higher melting temperature.

2.2. Macro parameters calculation and impurity distribution

The lattice parameter and the diffusion coefficients (by mean square displacement) calculation methods under isolated boundary conditions (separation of the internal region of nanocrystal and surface influence elimination) are described in detail in [5]. The only difference is that we excluded from mean square displacement calculation only those particles that came to the nanocrystal surface at least once during the simulation. Diffusion coefficients for comparison with experimental data we converted to the conductivity according to the classical Nernst-Einstein relationship:

$$\lim_{t\to\infty}\left[\frac{1}{N}\sum_{I}(\mathbf{r}_I(t)-\mathbf{r}_I(0))^2\right]=6\cdot D\cdot t$$
$$D=\frac{kT}{q^2N}\sigma \qquad (1)$$

where t is the simulation time, N the number of particles for MSD calculation, **r** the vector of particle coordinates, D is the self-diffusion coefficient, k the Boltzmann constant, T the temperature, σ the conductivity, q the ions charge, N is the concentration of ions. For a specific diffusion mechanism the following equality can be written:

$$\sigma T \approx D = D_0 \exp(-E_A/kT) \qquad (2)$$

where E_A is the activation energy for a specific diffusion mechanism.

Usually a system with a given X (impurity quantity) is created by replacing the required number of major Ce ions by impurity Gd ions in the original ideal CeO_2 lattice, and removing the "extra" oxygen ions. Regardless to the creation method of the simulated system, for the quantitative description of the resulting GdD we introduced the concept of "Gd complex". Two ions form a Gd complex when the first Gd ion is placed among the nearest neighbors of the second Gd ion, i.e. at a distance of $a/\sqrt{2}$ in the perfect fluorite lattice, where “a” is the lattice

parameter. Next Gd ion is considered to belong to the complex if it is located among the nearest neighbors of any of Gd, which forms this complex. The size of the complex we define as the number of Gd ions in the complex. The procedure for Gd complexes detection was performed by quickly cooling to 100K followed by relaxation during 10,000 MD steps, and cation coordinates were then obtained from average positions from next 1,000 MD steps.

2.3. Vacancy detection

To detect vacancies we should detect the oxygen sublattice nodes coordinates and to see if this nodes are occupied or free. Every N MD steps we averaged ion coordinates to avoid thermal oscillation. By the averaged coordinates of cations in the inner region of nanocrystal (which can rotate in vacuum) we built crystalline planes and detected the array of the ideal oxygen sublattice nodes IO. If a sphere with radius of 0.25 lattice parameter with a center at IO_J position contains none oxygen ion (which coordinates are averaged for N MD too) so this node IO_J is a vacancy. In this work we used the number of N = 1,000. Values N = 200, 500 demonstrated no differences at medium and low temperatures, but led to an increased computational cost, because the detection procedure had to perform more often.

At high temperatures for a specified number of steps N the oxygen ion can make several diffusion hops, which leads to some errors in the detection of impurity vacancies. Error can be estimated from the total number of vacancies in the inner region (bulk) of the nanocrystal, taking into account the appearance of intrinsic thermal vacancies at high temperatures. For KMKA12 potentials the vacancies quantity at T = 1800K exceeds the quantity of vacancies for low temperatures by 20%, and we suppose that up to that temperature the number of vacancies is obtained accurately. For Inaba potentials the total number of vacancies remains practically unchanged for all the simulated temperature, for T = 3100 K for this number exceeds the number of vacancies at low temperatures less then by

20%. Remind that the melting temperature of a nanocrystal of 39,150 ions with KMKA12 potentials set is T_m=2800 K, and a nanocrystal of 11,600 ions with Inaba potentials set has T_m=3300 K (see [5]).

To the detected vacancy we calculated the number of Gd ions in its nearest neighborhood. In the fluorite lattice we can define five vacancy types – with 0, 1, 2, 3 and 4 Gd ions in the nearest neighborhood of the oxygen sublattice node. For each temperature we obtained a vacancy fraction "n" as the number of vacancies of the given type divided by the total number of vacancies, and built a temperature dependence n(T).

To clarify the opportunity to obtain the equilibrium distribution of vacancies during simulations, we instantly froze a system of 39,150 ions with isolated GdD (potentials KMKA12) from 2000 K to 700 K (minimum temperature in this paper), and carried out simulation within 40 ns. The relaxation process of anion vacancies distribution of the given type is shown in Figure 1, where the vacancy fractions "n", surrounded by N (0, 1, 2, 3, 4) Gd ions and deviations σ_t of vacancy fractions n_t at time "t" from their equilibrium values n_∞ versus the simulation time are illustrated.

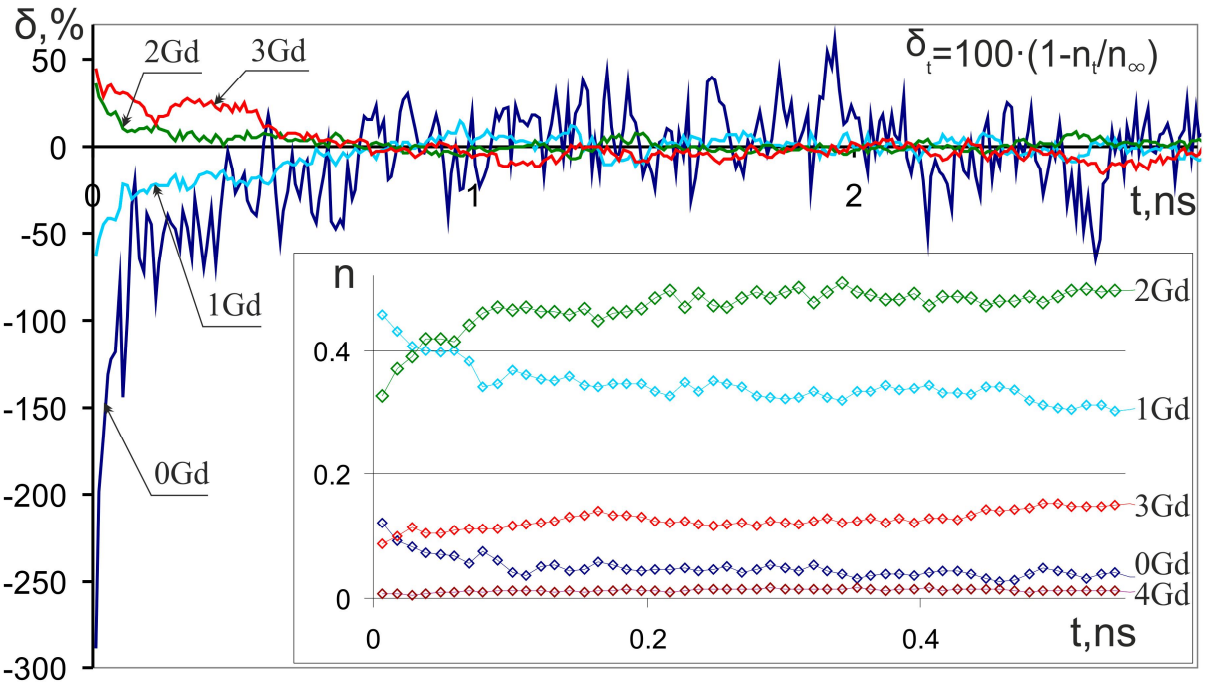

Fig. 1. Deviation of vacancy fractions surrounded by N Gd from its equilibrium values over the time. The inset shows the vacancy fractions dynamics over time, on a smaller time interval.

Fig. 1 shows that the relaxation process of anion vacancies of all types (values of deviations δ for 0Gd are great because the absolute number of vacancies surrounded by 0Gd are rather small) is almost finished at 3 ns. Despite this, to improve the statistics and accuracy for low temperatures of the order of 700 K the duration of the simulation was about 4,000,000 MD steps or 14 ns.

To reduce the computational cost during Gd complexes and vacancies detection we used chained cells, information about it can be found for example in [10].

Summary: Equilibrium distribution of anion vacancies during the MD simulation is realized. As long as from the technological point of view the procedure described above is the freezing of ceramics with the highest theoretically possible speed, there is a reason to believe that in real CGO ceramics the distribution of anion vacancies is equilibrium at any time.

3. MD simulation results and discussion

All simulations were performed for the two pair potentials sets. Data marked with the prefix «Inaba_» were obtained with potentials of Inaba et.al. [4]. MD results without any marks were obtained with KMKA12 potentials developed by us previously [5].

3.1. Gd distribution

MD limitation in our case is almost a complete immobility of the cations (excluding the thermal oscillation) at medium and low temperatures. Under periodical boundary conditions this immobility remains definitely and under isolated boundary conditions cations located in the surface layer can diffuse slowly. This makes it impossible to obtain the equilibrium distribution of Gd during MD simulation, especially in the bulk of nanocrystal, even at temperatures slightly below the melting temperature, for currently available simulation times

(microseconds). Therefore in the present work we specified the dopant cation distribution (GdD) when constructed the simulated system, and compared the GdD influence on the measured micro and macro parameters.

It is necessary to distinguish the **method** of impurity distribution and the distribution obtained in fact after applying this method. Method of distribution is the method of replacing the host cations (Ce) with the dopant cations (Gd) when creating the system. It should be emphasized that if we distribute isolated Gd ions, randomly one by one for example, we do not necessarily get the GdD at the end, which contains only Gd complexes consisting of one Gd ion, especially for large impurity concentration. So for high-defect system with a large X we can get an arbitrary number of Gd complexes of various sizes for nominally the same method of impurity distribution.

In this study we investigated three **methods** of distribution - isolated Gd, pair Gd and quad Gd. Distribution with a quad Gd was created so that in the nearest neighborhood of the anion (oxygen sublattice node) only Gd cations could be found. The last type of GdD was chosen for two reasons. First, this quad GdD is certainly artificial, and we should obtain the maximum deviation of macro parameters values from the other GdDs if GdD has a strong influence on macro parameters. Second, in spite of the large number of particles in the simulated system for isolated and paired GdD there were none oxygen sublattice node, surrounded only by the Gd ions, so it was not possible to find a vacancy fraction surrounded by four Gd or to obtain the temperature dependence of vacancies of this type.

Fig.2 shows the resulting dependence of the number of Gd complexes from it size for all three methods of GdD creation, for KMKA12 pair potentials set, before and after the simulation series, for the whole crystal (total) and only for the inner region (volume). The simulated system consisted of 39,150 ions.

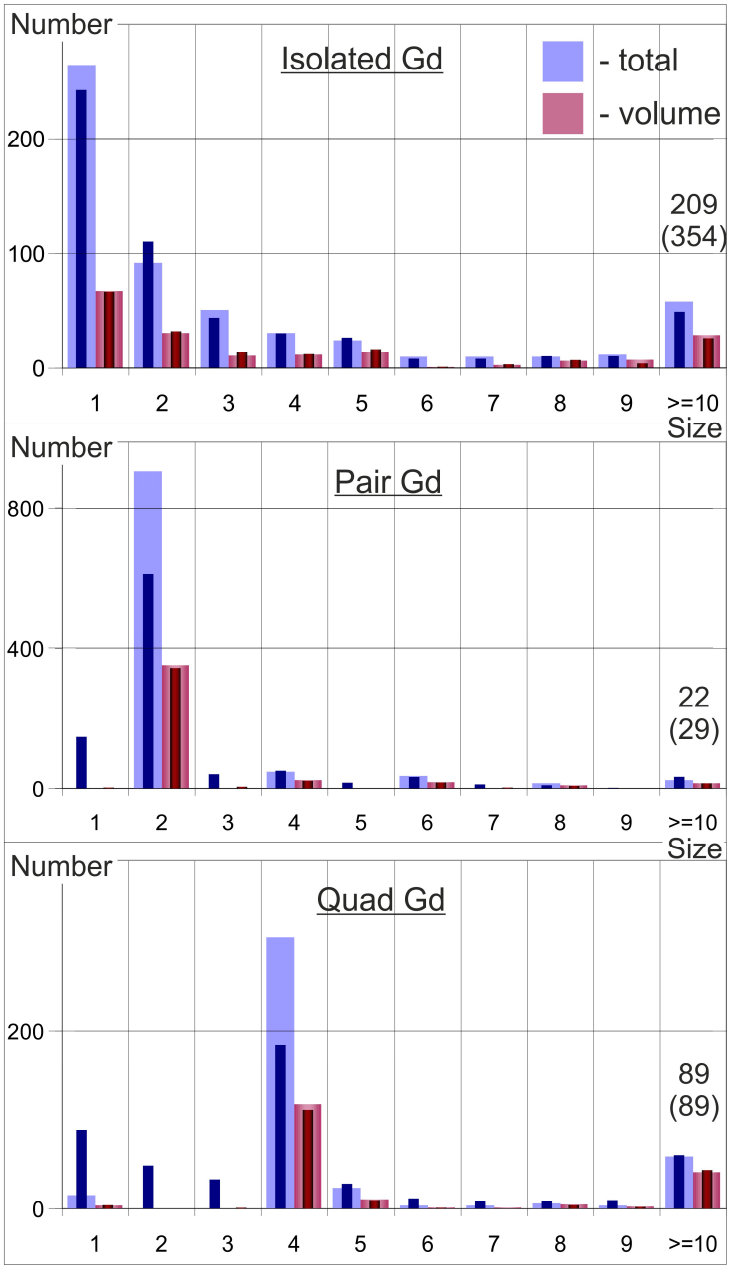

Fig.2. Number of Gd complexes versus the complex size (the number of Gd ions in the complex) for different GdD. The numbers on the right indicate the size of the largest complex in the crystal (in brackets - after the simulation series). "-total" means overal number of Gd complexed in a whole nanocrystal, and "-volume" means number of Gd complexes in the inner region of nanocrystal, which corresponds to the bulk of macrocrystal.

On the Fig. 2 for a given complex size the left bars refer to the total number of complexes, the right bars refer to the complexes, in which at least one of the Gd ions belongs to the interior region of the nanocrystal. Wide bars are obtained on the initially created system, the narrow bars obtained on the system after the simulation series.

Fig. 2 shows that the GdD remains unchanged for the inner region (bulk), and changes slightly on the surface. For the isolated GdD on the surface the number of single complexes decreases and the number of pair complexes increases, for the pair GdD on the contrary the number of single complexes increases and the number of pair complexes decreases. For the quad GdD the number of complexes with four Gd ions on the surface is significantly reduced and the number of complexes with one, two and three Gd ions is increased. For the isolated GdD a few large-sized complexes (about a hundred Gd ions) with a complicated elongated spatial form are observed. For the rest of GdD the number and size of large complexes are much smaller.

Based upon the dynamics of the impurity distribution on the surface and the presence of larger Gd complexes we suppose that in a real CGO ceramics Gd complexes with one and two Gd ions must co-exist in equilibrium, which confirmed despite the large measurement errors by EXAFS study [11]. And probably a large number of complexes with many Gd ions should present inside the bulk material, which is indirectly confirmed by experimental data [12].

With Inaba potentials set the systems of 11,600 ions with isolated and pair GdD were simulated. Gd complexes distributions for the respective GdD method are similar to that shown in Fig. 2. The tendency to form the mixture of isolated and pair Gd complexes on the surface of the nanocrystal is also observed.

3.2. Gd distribution influence on the lattice parameter

To clarify the effect of GdD on the lattice parameter (LP) of the simulated system for a given pair potentials set we have built the temperature dependences of the LP “a”, which are shown in Fig. 3. The same figure shows the temperature dependence of the LP deviation $\Delta a = a(\text{Pair Gd, Quad Gd}) - a(\text{Isolated Gd})$ for KMKA12 potentials. Unfortunately, we could not find in the literature the experimental data on the thermal expansion of the ceramic $Ce_{0.8}Gd_{0.2}O_{1.9}$, for comparison with our calculations.

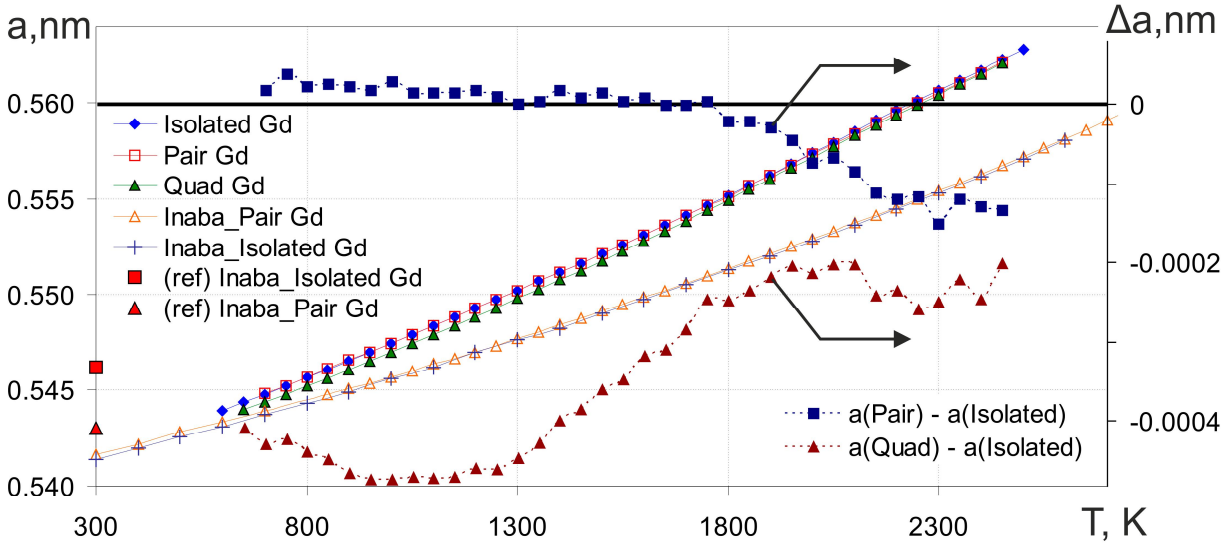

Fig.3. Lattice parameter versus simulation temperature. Data marked with (ref) were taken from [4]. On the right axis the absolute deviations of the lattice parameter of pair and quad GdD from isolated GdD are shown.

Approximation coefficients of the LP obtained during the MD simulations, fitted by the quadratic polynomial in the form of $a(nm) = \sum_{N=0}^{2} c_N \cdot T^N$, are shown in Table 1.

Table 1. Approximation coefficients for the temperature dependence of the lattice parameter of $Ce_{0.8}Gd_{0.2}O_{1.9}$ crystal for all GdD and interaction potentials sets.

Gd distribution	Interaction Potentials	c_0, nm	$c_1 \cdot 10^{-6}$, nm/K	$c_2 \cdot 10^{-10}$, nm/K^2
Isolated	KMKA12	0.53941	7.05809	9.43933
Pair	KMKA12	0.53924	7.37604	8.21005
Quad	KMKA12	0.53873	7.31766	9.26390
Isolated	Inaba	0.53987	4.88477	7.99389
Pair	Inaba	0.54051	4.07734	10.60169

Fig. 3 shows that the LP for isolated and pair GdD with KMKA12 potentials differs a little, for low and medium temperature the deviation does not exceed 0.00005 nm. Artificial system with quad Gd gives a much greater difference from LP of isolated Gd, nevertheless the maximum deviation does not exceed 0.0005 nm.

LP for isolated and pair Gd with Inaba potentials are practically identical for all the studied temperature range, as in the case of KMKA12 potentials. This result

differs greatly from those of Inaba [4] at 300 K, which are marked as "(ref)" and shown in Fig. 3. According to Inaba the LP for system with isolated Gd is much higher than that for a system with pair Gd, and the difference is 0.0032 nm. The LP value for the pair GdD obtained by Inaba is beyond the one obtained by us with Inaba potentials. Such an overestimation of LP for pure CeO_2 reported by Inaba was mentioned in our previous work [5].

Summary: GdD for a given set of potentials has almost no effect on the lattice parameter.

3.3. Oxygen diffusion coefficients with different GdD

Oxygen diffusion coefficients D in Arrhenius coordinates and their deviations |ΔD|/D in percentage terms for KMKA12 potentials for all simulated temperatures are shown in Fig. 4.

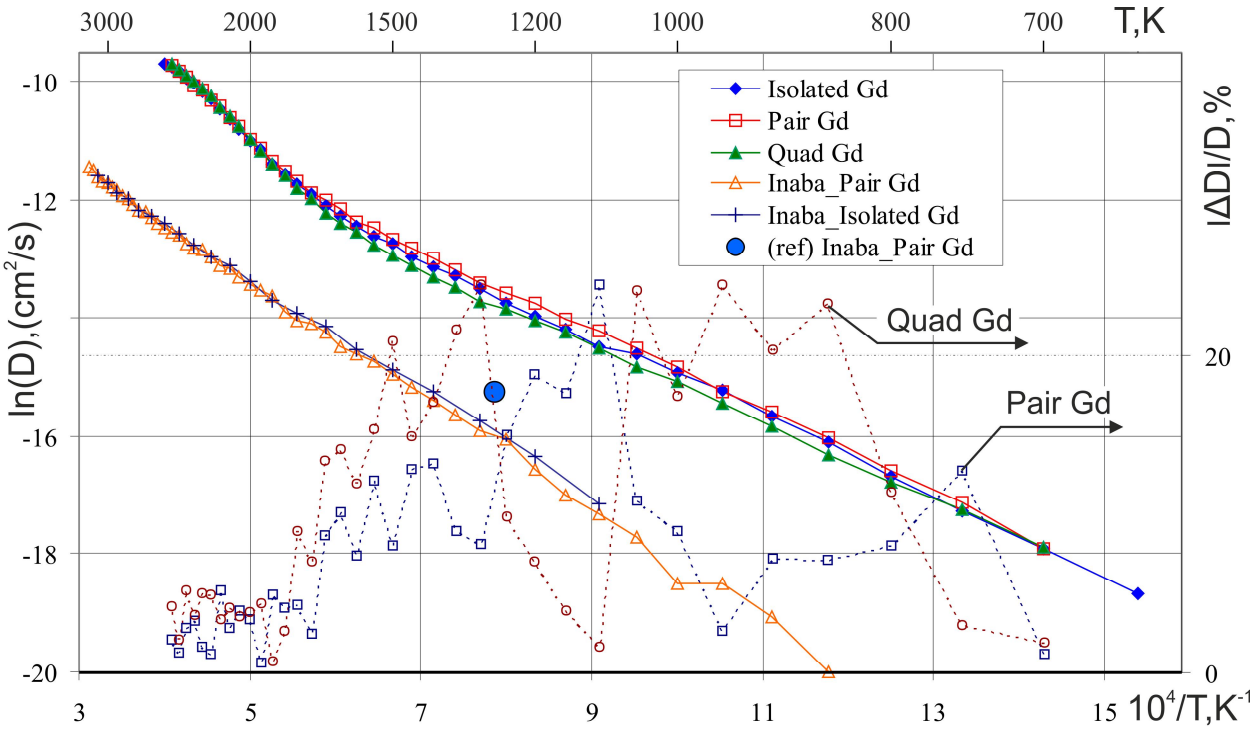

Fig.4. Oxygen diffusion coefficients with different GdD. Data marked with (ref) were obtained from [13]. On the right axis the modules of relative deviation of the diffusion coefficient with specified GdD from diffusion coefficient with isolated GdD are shown, for KMKA12 potentials set.

It follows from the data in Fig. 4 that for various GdD the diffusion coefficients differ slightly between themselves, for the given potentials set (in spite of a significant difference in the values for Inaba and KMKA12 potentials sets). Diffusion coefficient deviations (|ΔD|/D, %) are maximum for medium and low temperatures, but do not exceed 25%. The value of diffusion coefficient obtained by Hayashi [13] with Inaba potentials (marked as "ref" in Fig. 4) is much higher than values we obtained with Inaba potentials for both GdD.

On the diffusion coefficient curve obtained with KMKA12 potentials the bend, corresponding to the transition from impurity to intrinsic disorder (T~1800K), is distinctly observed with increasing temperature, and then the next bend of superionic transition (T~2200K) is presented. For Inaba potentials superionic transition bend is not observed even for pure CeO_2, and the transition to intrinsic disorder is almost unnoticeable.

Summary: GdD has insignificant influence on the anion diffusion coefficient for a given set of interaction potentials.

3.4. Comparison of calculated diffusion coefficients with experimental conductivity

In the literature a lot of data on the ionic conductivity of CGO ceramics are presented, and practically no data corresponding to oxygen diffusion coefficients are available, which is related with a certain experimental difficulties. So, for comparison with the MD calculated diffusion coefficients we should separate the diffusion in the grain (bulk) and the grain boundary, which is impossible in the SIMS experiments, but is quite easy in ionic conductivity measurements by impedance spectroscopy.

The results of our MD calculations of the anion diffusion coefficients at medium and low temperature we converted to conductivity in accordance with (1). The only experimental oxygen diffusion coefficients we have found, obtained by Manning et al. [14], we converted to conductivity in the same manner. In conversion of the calculated diffusion data into conductivity we used the actual

MD charge of oxygen. In conversion of the experimental values [14] we used the formal oxygen charge equals to "-2". As follows from (1) the decreasing of the oxygen charge leads to a decrease in conductivity. All conductivity values are given in Fig. 5.

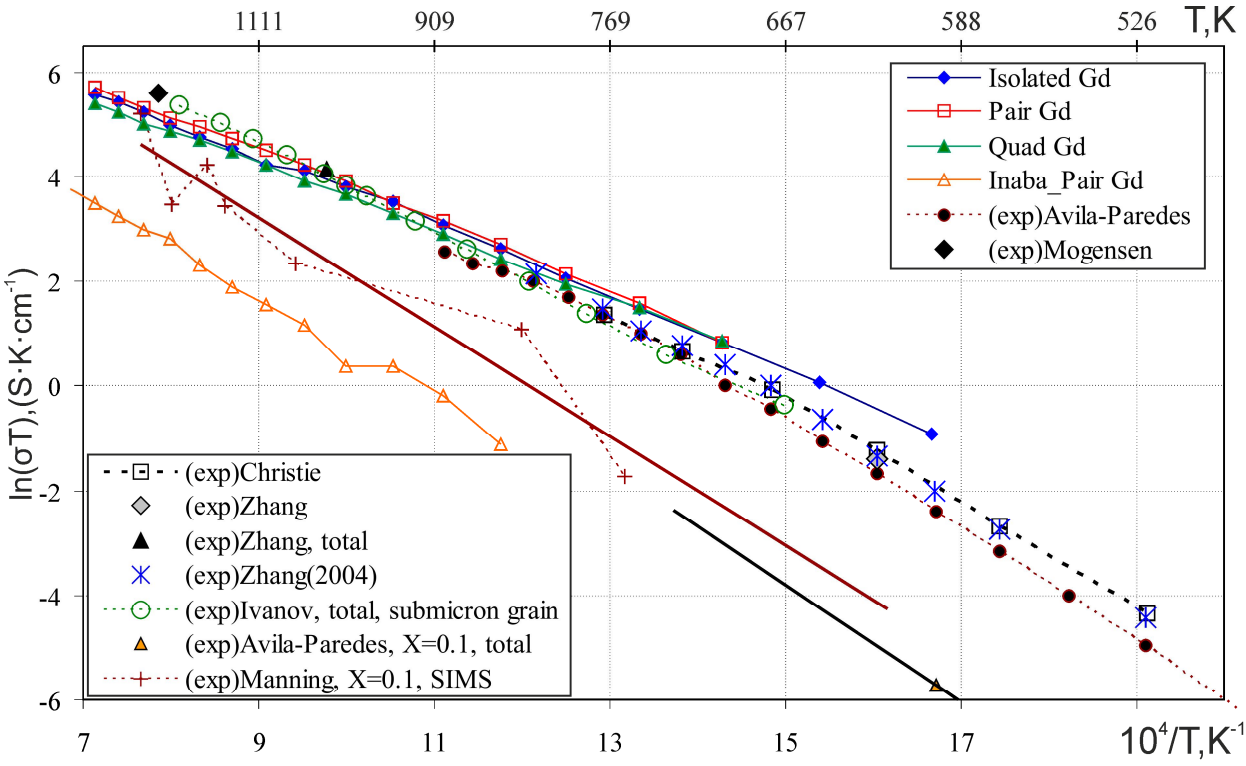

Fig.5. Calculated by the MD and experimental (with prefix (exp)) conductivities in Arrhenius coordinates. References to the experimental data are given in the text. Experimental data labels without any specification corresponds to the bulk conductivity for X = 0.2. The "total" in the label text specify the total conductivity.

Calculations results of the anion diffusion in the inner region of the nanocrystal should be compared with bulk diffusion and conductivity. Experimental data on the bulk conductivity of $Ce_{0.8}Gd_{0.2}O_{1.9}$ crystals were taken from Avila-Paredes [15], Mogensen [16], Christie [17] and Zhang [18]. Grain boundaries influence on the conductivity decreases with increasing temperature, and according to Zhang [19] total conductivity (marked as “(exp) Zhang, total” in Fig.5) is approximately equal to the bulk conductivity. In [17] it is shown that when a size of the grain is decreased the grain boundary resistance decreases. Total conductivity "Ivanov, total, submicron grain" [20] of the ceramics, which has a grain size of about 250nm, is almost identical in magnitude to the bulk

conductivity. Samples of this ceramics with submicron grains, produced by Ivanov et al., we have investigated in helium thermal desorption experiments, which will be discussed later in 3.7.

Oxygen isotopes diffusion coefficients "Manning, X=0.1, SIMS" [14] are characterized by large dispersion, which is typical for experimental methods of diffusion coefficients measurement. It were obtained with the samples with X = 0.1, and bring, in particular, to demonstrate the correctness of the Nernst-Einstein relation (1) using. The depth of the oxygen isotope profile is 0.07cm, the average grain size for typical CGO ceramics can be estimated as 10μm = 0.01cm (see for example [17]) – so, it can be assumed that in the SIMS experiments the total effective diffusion was measured (in the bulk and in the grain boundary), and it should be compared with the total conductivity. Data on the total conductivity for CGO ceramics with X=0.1 were obtained from [15] and are marked on the Fig.5 as "Avila-Paredes, X=0.1, total". There are three conductivity points that are fitted well by a straight line, and two points are not shown to not to reduce the graph scale. Extrapolation of these conductivity data to high temperature acceptably coincides with the extrapolation of the diffusion data to low temperature.

It follows from the data in Fig. 5 that the absolute values of the conductivities calculated by MD with the KMKA12 potentials for all GdD are close to the experimental ones. Diffusion coefficients with Inaba potentials look underestimated and are even lower than the total conductivity experimental data for the of crystals with X = 0.1. On the Fig. 5 it can be seen a low temperature bend (650 K - 750 K) on all the bulk conductivity experimental curves, which will be discussed later.

Calculated and experimental diffusion (conductivity) activation energies E_A, obtained by (2) for medium temperatures above 750 K, are given in Table 2.

Table 2. Calculated by MD and experimental activation energies.

Source	E_A,eV	Source	E_A,eV	Source	E_A,eV
IsolatedGd$^+$	0.58	Inaba_PairGd*	0.81	Ivanov [20]	0.74
PairGd$^+$	0.58	Avila-Paredes	0.71	Avila-Paredes	0.96

		[15]		[15], X=0.1	
QuadGd^{+}	0.56	Christie [17]	0.63	Manning [14], SIMS, X=0.1	0.90
Inaba_IsolatedGd*	0.77	Zhang [18]	0.69		

($^{+}$) means calculation with KMKA12 potentials, (*) – calculation with Inaba potentials, and other data are experimental.

The calculated activation energies for the different GdD for the given potentials set are practically the same, which again suggests a weak GdD influence on the macro parameters. The experimental activation energies for the bulk conductivity (Avila-Paredes, Christie, Zhang) and for the total conductivity of submicron ceramic (Ivanov) correlate well with each other, this value can be taken as 0.7 eV, and it exceeds by 0.1 eV the MD activation energy of approximately 0.6 eV for KMKA12 potentials. In turn, the activation energy for the Inaba potentials exceeds this experimental estimation by 0.1 eV, though the absolute MD calculated values of the conductivity are much lower.

In [17] Christie gives estimation of the diffusion activation energy equal to 0.9eV for all the studied temperature range (6 points in the range of 250-500 ˚C) for CGO ceramics with a grain size of ~ 1μm. However, during his data processing we clearly saw the bend; the activation energy determined by us for the entire temperature range is equal to 0.80 eV, and the only high-temperature points give us the value of 0.63 eV.

3.5. Distribution of the anionic impurity vacancies for different Gd ions distributions

Temperature dependences of the vacancy fractions n_K with various number K=(0, 1, 2, 3, 4) of Gd ions in the nearest neighborhood, for different GdD with KMKA12 potentials, are shown in Fig. 6.

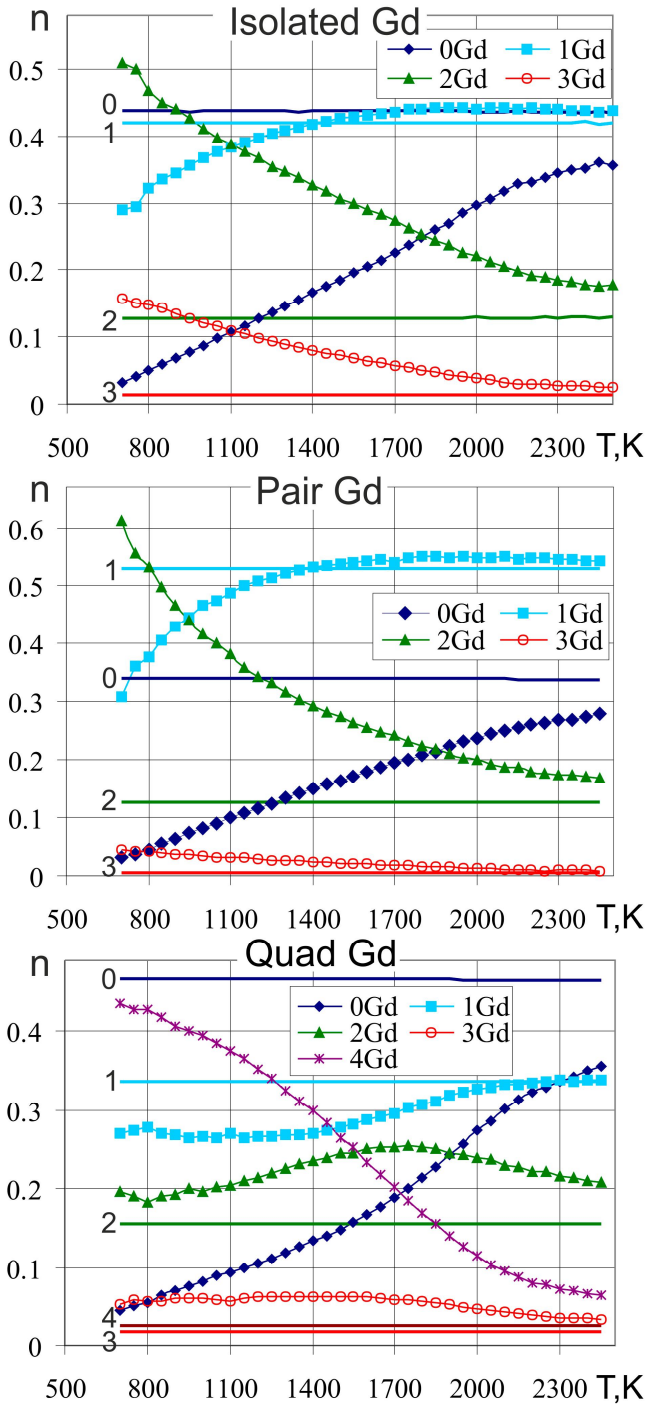

Fig. 6. Temperature dependences of the vacancy fractions n_K with K Gd ions in the nearest neighborhood. Horizontal lines show temperature dependences of the anion sublattice nodes fractions, surrounded by K Gd ions (marked by the number on the left of line).

In the inner region of the simulated nanocrystal of 39,150 ions about 400 impurity vacancies and about 8,000 anionic sublattice nodes were detected. To obtain the value of the vacancy or node concentration with K Gd ions in the nearest neighborhood the corresponding vacancy or node fraction should be multiplied by

the concentration of total number of vacancies or nodes, which can be easily determined for $Ce_{1-X}Gd_XO_{2-X/2}$ crystal for a given X.

From Fig. 6 a tendency can be seen that coincides with the general thermodynamic concepts (see for example [21]), which consists in the fact that with increasing temperature the impurity-vacancy complexes with a large number of Gd ions dissociate, or, in other words, vacancies moves to the oxygen sublattice nodes with the lesser number of Gd ions in the nearest neighborhood. For isolated and pair GdD vacancy fractions surrounded by 2 and 3 Gd ions decrease and vacancy fractions surrounded by 1 and 0 Gd increase with increasing temperature. For quad GdD vacancy fractions surrounded by 1 and 2 Gd increase first, since when vacancy with 4 Gd jumps in any direction near it at least two Gd ions can be found. If in the case of quad GdD we convert vacancy and oxygen sublattice nodes fractions surrounded by 4 Gd ions into concentrations, we find that for low temperatures (T~700 K) almost all the anion sublattice nodes with the 4 Gd are occupied by the vacancies.

Vacancy fractions for low and medium temperatures are well approximated by the straight line in the Arrhenius coordinates, similar to (2). We suppose that the slope of that line determines the formation energy of vacancies of the given type (surrounded by K Gd ions). Formation energies of the vacancies of all types for all GdD are shown in Table 3.

Table 3. Formation energies E_K of vacancies, surrounded by K Gd ions.

Gd distribution	E_0(0Gd),eV	E_1(1Gd),eV	E_2(2Gd),eV	E_3(3Gd),eV	E_4(4Gd),eV
Isolated Gd	0.195	0.050	-0.044	-0.058	---
Pair Gd	0.196	0.069	-0.080	-0.070	---
Quad Gd	0.129	-0.007	0.032	0.013	-0.022

"---" – data not shown due to lack of nodes surrounded by 4 Gd.

The positive formation energy means that the vacancy fraction of this type increases with increasing temperature.

Impurity vacancies present in the crystal as a result of electroneutrality requirement, and their formation energy is identically zero (they are present, and their number does not depend on temperature). Effective total vacancy formation energy we define as:

$$E(T) = \sum_{K=0}^{4} n_K(T) \cdot E_K \qquad (3)$$

where $n_K(T)$ is the vacancy fraction, surrounded by K Gd ions, for the given temperature T, E_K the formation energy of vacancy of the given type. This effective energy value is almost zero for low and medium temperatures.

3.6. Distribution of the anionic impurity vacancies with Inaba potentials

Vacancy detection results with Inaba potentials are brought in a separate section because on the microscopic level of defect investigation Inaba potentials gives unphysical results and differ a lot from results with KMKA12 potentials. These results are interesting from a methodological point of view, as a demonstration of the potentials influence on macro and micro parameters. Vacancy distributions in a system of 11,600 ions with Inaba potentials are shown in Figure 7.

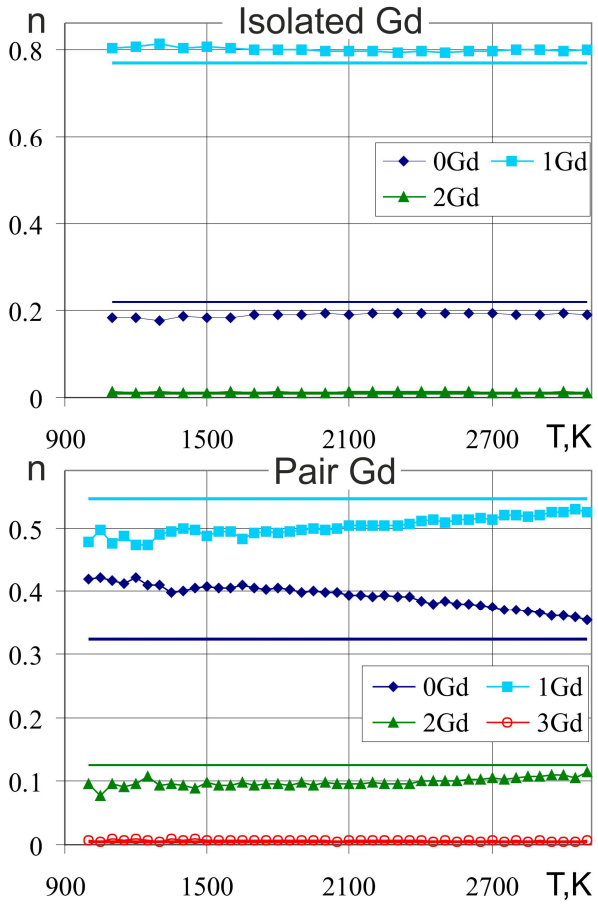

Fig.7. Inaba interaction potentials. Temperature dependences of the vacancy fractions n_K with the K number of Gd ions in the nearest neighborhood.

In this case, the inner region of the nanocrystal contained about 140 impurity vacancies and approximately 2,750 anionic sublattice nodes. For isolated GdD the vacancy distribution is essentially independent of temperature, while the pair GdD demonstrates an inverse to KMKA12 case behavior - while the temperature is increased the vacancy fractions surrounded by 1 and 2 Gd increase, and vacancy fraction surrounded by only Ce cations (0 Gd) decreases. Such behavior is contrary to the general thermodynamic concepts. The coincidence of the vacancy fraction of a given type with the corresponding anion sublattice nodes fraction means that the vacancies are distributed across the nodes uniformly.

We suppose that such behavior can be explained by the pair interaction potentials, which are shown in Fig. 8.

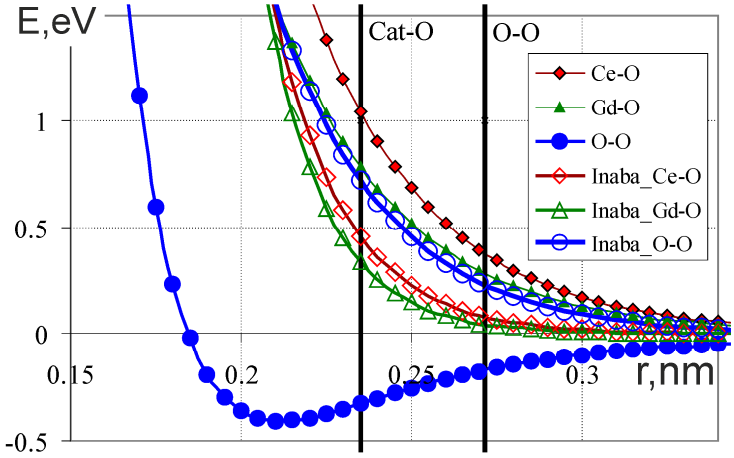

Fig.8. Overall interaction energy (Coulomb plus non-Coulomb) versus distance between ions. The vertical lines indicate the approximate distance between the "cation-oxygen" and "oxygen-oxygen" pairs.

In the case of Inaba potentials the repulsive energy of the "oxygen-oxygen" pair exceeds the repulsion energy of other "oxygen-cation" pairs, so oxygen ions push each other in the nearest vacancy, ignoring nearest cationic neighborhood of the vacancy. Minimum of the O-O potential is shifted to the right by a distance of 0.475 nm, with a value of only -0.00088 eV. Such "rigidity" of the oxygen-oxygen potential, apparently, causes both low diffusion coefficients values and almost unnoticeable bend on the diffusion coefficients curve, corresponding to the transition from impurity to intrinsic disorder at high temperatures.

3.7. Investigating of the helium dissolution mechanism in CGO ceramics

Consider the experimental results obtained by the low-temperature helium defectoscopy method for the samples of $Ce_{0.8}Gd_{0.2}O_{1.9}$ ceramics. In this method we saturate the sample with helium at a given pressure and temperature, then degas it in vacuum and with a mass spectrometer determine by the number of released helium, and, respectively, the concentration of helium dissolved in the sample. Helium defectoscopy method is described in detail in [22]. Typically, for a given temperature with increasing of helium saturation pressure the dissolved helium concentration goes on a "plateau". From a consideration of the thermodynamic

equilibrium conditions in the “gas-imperfect crystal” system, for one defect type for the dissolution of the gas atoms, this relationship can be written as:

$$C(P) = \frac{C_V^* \Gamma P}{1 + \Gamma P} \qquad (4)$$

where C is concentration (solubility) of helium, which depends on the saturation pressure P, C_V^* the helium concentration on the "plateau" or concentration of all available positions to dissolution, Γ the value weakly depends on the pressure. Helium solubility goes on a "plateau" when the helium atoms occupy all possible positions for dissolution. Thus, we can get the numerical value of the concentration of a certain defects type in the crystal, and to determine the type of these defects.

Previously we could demonstrate the efficiency of helium defectoscopy method in determination of the thermal vacancies concentration in LiF [23] and in determination of the vacancy clusters concentration in the Pd with sub microcrystalline structure [24]. In the case of LiF the "plateau" value increases with increasing temperature, and in the case of Pd "plateau" value remains unchanged with temperature, the temperature affects only the slope of the solubility curve.

Applying the method of helium defectoscopy to $Ce_{0.8}Gd_{0.2}O_{1.9}$ system at low temperatures we expected to fill all the impurity vacancies (which concentration is constant) at some saturation pressure. However, though we discovered "plateau" on the helium solubility, the concentration of dissolved helium on a "plateau" increases with the saturation temperature. The characteristic value of the “plateau”, for example $2 \cdot 10^{19}$ cm^{-3} for the saturation temperature T=773 K [25], by two orders of magnitude lower the impurity vacancies concentration, which is about $2.5 \cdot 10^{21}$ cm^{-3} for X=0.2.

Possible positions for the dissolution of helium atoms in the CGO ceramics are point defects (for discussed temperatures it is only impurity vacancies), extended defects - dislocations and grain boundaries, volume defects, and technological impurities (Ca, Na, Fe). The concentrations of all these defects do **not depend** on the temperature. The concentration of any of the above types of

defects exceeds the specified characteristic value of the helium solubility on the "plateau" and may serve as dissolution positions, but no one type of defects can not explain the rise of the number of dissolution positions with increasing temperature. At the same time the characteristic of experiment was so that the weakly bound helium (in pores for example) quickly left the sample, and was not included in the resulting solubility.

We suggest the following model: helium atoms dissolve only in those vacancies in the nearest neighborhood of which there are four cerium cations or none gadolinium cations. In Fig.9 the concentration of vacancies, surrounded by 0 Gd ions, obtained with KMKA12 potentials, and the helium concentration on the "plateau" from [25] are given.

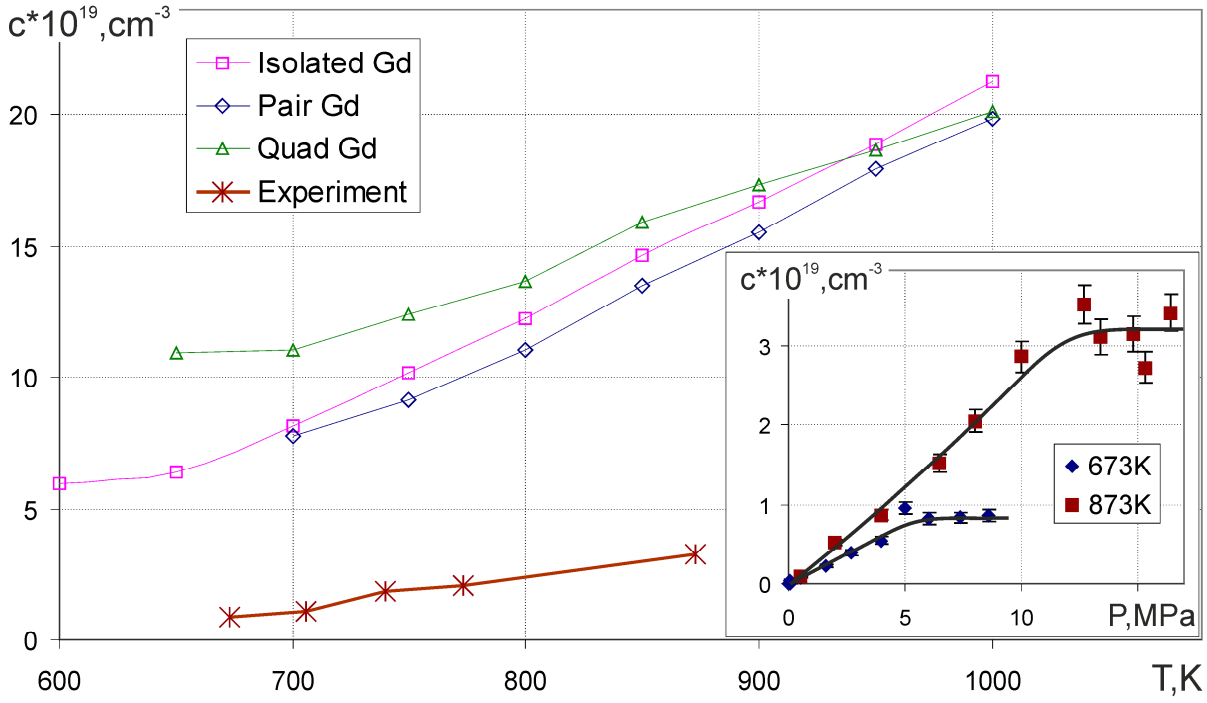

Fig. 9. The temperature dependence of the helium concentration on the "plateau" (positions for dissolution) and the concentration of vacancies surrounded only by cerium cations for different GdD. The insert shows the experimental results of helium defectoscopy method – the examples of helium solubility isotherms (dissolved helium concentration versus saturation pressure).

At low temperatures the difference of the experimental and calculated concentrations is less than an order. At that the concentrations of all possible positions for helium dissolution (crystal defects) exceeds the experimental helium concentration on the "plateau" by 2-3 orders of magnitude. Experimental formation

energy of the positions for helium dissolution is (0.33 ± 0.04) eV and exceeds the calculated by MD formation energy equals to 0.2 eV.

The reason for the helium dissolution in vacancies surrounded only by cerium cations is probably the pair interaction potentials of cations and helium atoms. It can be assumed that the Gd cation pushes helium atom out from vacancy, and the cerium-helium potential has a considerable pit in the equilibrium position of helium in vacancy. First-principles calculations should clarify this assumption, and it will be done in future work.

Summary: The assumption that helium atoms dissolve in vacancies, surrounded only by cerium ions, was discussed. MD results qualitatively reproduce the experimental results of helium defectoscopy method, but not give the absolute coincidence of helium solubility and dissolution energy values.

3.8. Low-temperature bend in experimental bulk conductivity

In Fig. 5 the bend on every experimental curve for the bulk conductivity (by Zhang, Avila-Paredes and Cristie) can be observed. Zhang and Avila-Paredes detected and discussed this bend and the bend in bulk conductivity given by Cristie we observed when processed his data. This bend the authors discussed in the terms of dissociation of "impurity ion-vacancy" complex with increasing temperature, and this reversible association-dissociation reaction in Kröger notation is written as:

$$(\mathrm{Gd_{Ce}V_O})^{+} \rightarrow \mathrm{Gd_{Ce}^{-}} + \mathrm{V_O^{2+}} \qquad (5)$$

Let’s determine the temperature dependence of the number of "free" vacancies, not associated with the impurity ions. Suppose that "free" vacancy is generated as a result of reaction (5), although in the fluorite lattice the vacancy in $(2\mathrm{Gd_{Ce}V_O})^{x}$ complex near two Gd ions, in addition to hopes in 4 directions with $(\mathrm{Gd_{Ce}V_O})^{+}$ complex formation, can jump in two directions and become "free." Consider only the impurity disorder region, without thermal anti-Frenkel defects. Solve the system of three equations - reversible dissociation reaction of the complex (5),

electro neutrality condition and total concentration of impurity ions, which for a given crystal is fixed and known:

$$\begin{gathered}\left[Gd_{Ce}^{-}\right]\left[V_O^{2+}\right]=K_a\left[\left(Gd_{Ce}V_O\right)^{+}\right],\ K_a=C\cdot\exp(-E_{asn}/kT)\\ 4\left[V_O^{2+}\right]+\left[\left(Gd_{Ce}V_O\right)^{+}\right]=\left[Gd_{Ce}^{-}\right]\\ \left[Gd_{Ce}^{-}\right]+\left[\left(Gd_{Ce}V_O\right)^{+}\right]=\left[Gd\right]\end{gathered} \tag{6}$$

where K_a is a reaction constant, E_{asn} the complex association energy. Variables in the square brackets are the atomic fractions, equal to the number of defects divided to the number of nodes N_L of the corresponding sublattice:

$$\left[X_s\right]=N_X/N_{LS},\quad N_{LCe}=2N_{LO} \tag{7}$$

Solution of the system (6) is the temperature dependence of the “free” vacancy concentration:

$$\left[V_O^{2+}\right]=\left(\frac{\left[Gd\right]+4K_a}{8}\right)\left(-1+\sqrt{1+\frac{16K_a\left[Gd\right]}{\left(\left[Gd\right]+4K_a\right)^2}}\right) \tag{8}$$

The extreme cases of this solution are the cases of high temperatures or low impurity concentrations, when all vacancies are “free”:

$$K_a>>\left[Gd\right]:\ \left[V_O^{2+}\right]\approx\frac{\left[Gd\right]}{4}=\left[V\right] \tag{9}$$

where [V] is the concentration of all impurity vacancies, and the cases of low temperatures or high impurity concentration, when practically all vacancies are associated with impurity ions:

$$K_a<<\left[Gd\right]:\ \left[V_O^{2+}\right]\approx K_a \tag{10}$$

At the vacancy diffusion mechanism the diffusion is determined by the product of independent factors - the concentration of "free" vacancies and the probability of anion hopping to vacancy:

$$\sigma T\approx D=\text{const}\cdot\left[V_O^{2+}\right]\cdot\exp(-E_m/kT) \tag{11}$$

where E_m is the migration energy. Equations (10) and (11) allows to determine the association energy of the complex as the difference of activation energies before and after the bend on the conductivity or diffusion curves (Fig. 5), if we **exactly**

know that this bend is related to the dissociation of complexes like (5), and the extreme cases (9) and (10) are satisfied.

"Free" vacancies in the terms of the MD calculations correspond to vacancies, surrounded only by Ce ions, or with 0 Gd ions. Let's reduce the expression (8) to the vacancy fraction n_0 with 0 Gd ions in the nearest neighborhood:

$$n_0 = \frac{\left[V_O^{2+}\right]}{\left[V\right]} = 0.5 \cdot \left(1 + f(T)\right)\left(-1 + \sqrt{1 + \frac{4f(T)}{\left(1 + f(T)\right)^2}} \right),\ f(T) = C \cdot \exp(-E_{asn}/kT) \quad (12)$$

We assume that in Fig. 5 region after the bend (above ~ 700K) refers to the strong defect association and the concentration of "free" vacancies should be described in the approximation (10). Bend on the conductivity curves is not associated with the dissociation of the complexes (5), although the authors Zhang and Avila-Paredes surely had no reason to think otherwise when processed their experimental data. Accordingly the experimental conductivity activation energy after the bend is the sum of the migration energy E_m and the vacancy association energy E_{asn}. To confirm this assumption we adduce three arguments:

1) The concentration of "free" vacancies in helium defectoscopy experiments in the region of complete complexes dissociation, according to the equation (9), should be constant and close in magnitude to the concentration of all impurity vacancies in the crystal. However, the concentration curve of "free" vacancies in Arrhenius coordinates (Fig.9) is linear, well approximated by the solution (10), and the absolute concentration values are of 2-3 orders of magnitude lower the concentration of all impurity vacancies.

2) The results of MD simulations (Fig. 6) show that for all GdD the vacancy fraction n_0 with 0 Gd ions in the nearest neighborhood does not exceed 0.4 up to the melting point, which indicates the strong association of vacancies with impurity cations. Moreover, the available nodes fraction in anion sublattice with 0 Gd ions in the nearest neighborhood does not exceed the value of 0.5, which makes the simultaneous distribution of all impurity vacancies in these positions extremely unlikely.

3) On the conductivity curves of the best studied crystals, such as NaCl doped with Mn (0.0325% mol) [26] and CaF_2 doped with Na (0.0007% mol) [27], the bend reliably concerned with the association-dissociation of "impurity ion-vacancy" complexes is observed. For both crystals the bend temperature is about 0.5 melting temperature. For crystal with 20% of dopant studied in this work it is hard to expect full dissociation of the complexes at temperatures of about 0.3 melting temperature after the bend, which is shown in Fig. 5.

To determine the influence of impurity concentration X in the simulated system on the dissociation rate of the complexes "impurity ion-vacancy" the MD simulations of nanocrystals with X = (0.1, 0.05, 0.01) with pair GdD and the number of particles of about 12,000 were carried out, with KMKA12 potentials. Temperature dependences of vacancy fraction with 0 Gd ions in the nearest neighborhood for described above systems and for system with X=0.2 with pair GdD (from Fig. 6), as well as the approximation of these data by equation (12), are shown in Fig. 10.

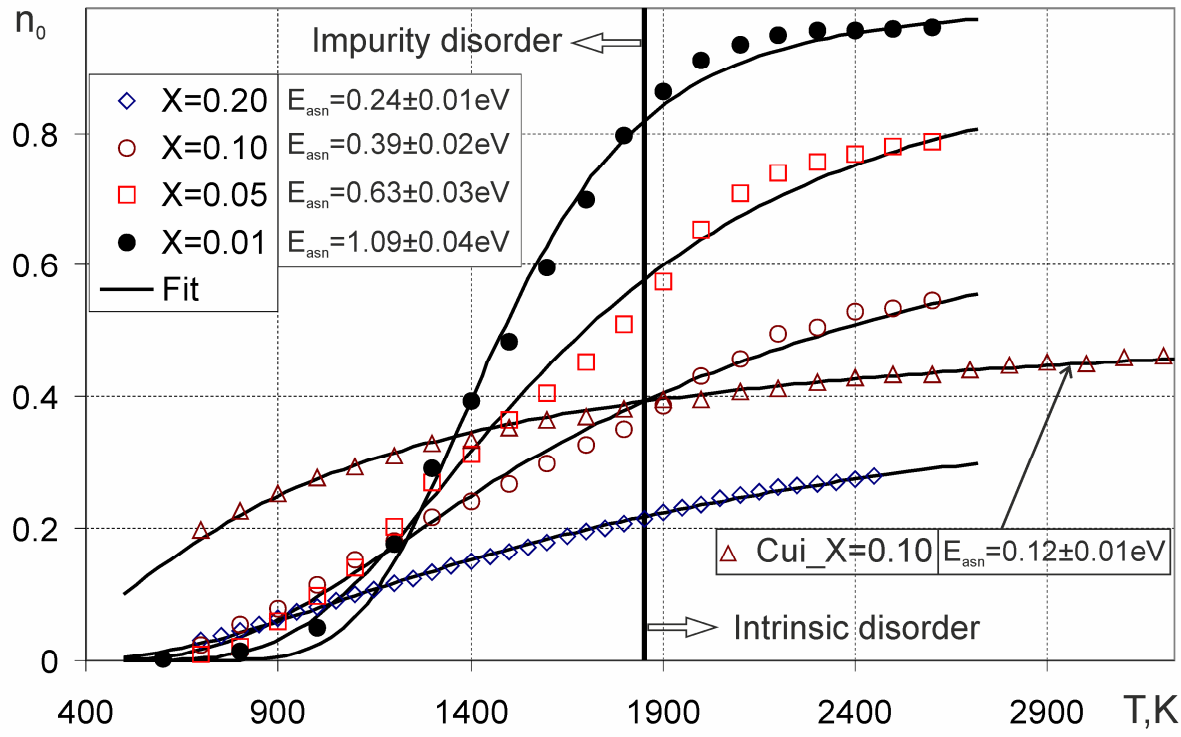

Fig. 10. Temperature dependences of the "free" vacancies fraction with 0 Gd ions in the nearest neighborhood for $Ce_{1-X}Gd_XO_{2-X/2}$ systems with different X. Approximation of calculated data according to the equation (12) is shown by the solid line. Vertical line indicates the approximate

temperature where transition from impurity to intrinsic disorder takes place, according to anion diffusion data (except for the simulation results with Cui potentials).

Simulation results for system consisted of 11,800 ions with pair GdD with potentials developed by Cui et al. [28] and approximation of these results by equation (12) are shown for comparison in Fig. 10. These potentials were obtained from quantum-chemical calculations and were fitted in the rigid ion approximation with formal ion charges. Cui potentials look similar to KMKA12 potentials (Fig. 8), namely the oxygen-oxygen potential has an even deeper minimum of about (-0.77) eV at a distance of 2 Å. The melting temperature of above crystal with Cui potentials equals to T = (4350±50) K and the specific volume change at melting is $\Delta V/V$ = (13.6±0.2) %. Despite of the lower formation energy of "free" vacancies with Cui potentials the behavior of the vacancy temperature dependence coincides with the corresponding dependence calculated with KMKA12 potentials. Vacancy fraction surrounded only by Ce ions increases with increasing temperature and vacancy fractions with at least one impurity Gd ion in the nearest neighborhood decrease.

The above shows that at low temperatures the vacancies tend to associate with impurity ions. But Cui et al. in their study [28] concluded that "the vacancy opts not to be adjacent to any cations" and "the cation-vacancy cluster may not be stabilized". Cui et al. made this conclusion based upon the calculations of oxygen coordination number (by integrating the first peak of Ce-O and Gd-O pair correlation functions) for different impurity concentrations X at a temperature of T = 300 K. We suppose that the distribution of impurity vacancies in Cui et al. calculations was not equilibrium, and as the initial distribution of impurity ions and vacancies was random the resulting pair correlation functions showed no tendency of association of the vacancies with impurity ions. Indeed, the vacancy relaxation process concerns to the diffusion of anions and is thermally activated, and our calculations show that for KMKA12 potentials at T = 700 K equilibrium is reached during 3 ns (Fig. 1). Maximum simulation time mentioned in the Cui et al. article was 0.5 ns and the equilibrium for this time at T = 300 K is unachievable.

It follows from the data in Fig. 10 that even for the minimum studied X vacancies are mainly associated with impurity cations up to 1500K. Now, taking into account vacancy association, we can determine the migration energy E_m of anions. Experimental migration energy we define as the difference between the conductivity activation energy (Fig. 5, above the low-temperature bend) and the formation energy of “free” vacancies from helium defectoscopy data at the same temperatures (Fig. 9), and calculated one as the difference of the corresponding energies obtained by MD. Migration energies are given in Table 4.

Table 4. Experimental and calculated anion migration energies.

Author	E_m, eV
Avila-Paredes [15]	0.38
Zhang [18]	0.36
Christie [17]	0.3
MD (Pair GdD, KMKA12)	0.34

Bend on the conductivity curves in Fig. 5 perhaps concerned to the association of "free" vacancies with large impurity clusters - regions within the grains with a high local dopant concentration. In the work [25] on the concentration curve of helium on the "plateau" (in Arrhenius coordinates) the bend can also be seen, although when we prepared this article we had no reason to fit the data otherwise than a straight line. The coincidence of the bend temperature on conductivity and helium concentration curves, of about 670-770K, suggests that the bend mechanisms are the same in both cases and concerned with the "free" vacancies.

Probably, in real crystals the more complicated GdD than studied in this paper is existed, and the bend on the curves of experimental conductivity and helium solubility is determined by the interaction of vacancies and these more complicated Gd complexes. Indirect evidences of this assumption can be the work [29], in which the authors obtained the ratio of Ce and Gd ions equals to 1:1 in the first surface layer (local X=0.5), and the work [12], in which the authors found

"microdomains" in the grain - perhaps the area with high local concentration of impurities. The study of such large complexes is beyond the scope of this paper.

Summary: In the systems with high dopant concentration (X=0.2) vacancies are predominantly associated with the impurity ions almost to the melting temperature. Temperature dependence of these "free" vacancies is well approximated by the solution (12). The bend on the conductivity curves is not concerned with the dissociation of the complexes "impurity ion-vacancy", but probably with a dissociation of vacancies from the regions of the crystals with a high local dopant concentration.

4. Conclusions

1) The simulations of nanocrystals with different dopant distribution with two pair potentials sets were carried out. It is shown that for a given potentials set the dopant distribution does NOT affect the calculated macro parameters, namely the lattice parameter and the anion diffusion coefficient. High-speed MD on GPU allowed us to simulate nanocrystals of about 40,000 ions within 0.1 ms. A good agreement between experimental and calculated conductivities for KMKA12 potentials set was obtained.

2) Temperature dependences of the of the vacancy fractions with different number of Gd ions in the nearest neighborhood, for various Gd distributions, were calculated. Formation energies of the vacancies of all types with KMKA12 potentials were obtained. Calculated formation energy of vacancies surrounded only by Ce ions (0.24±0.01) eV is close to the value of formation energy of “free” vacancies (0.33±0.04) eV obtained from helium defectoscopy experiments.

3) The supposition that in CGO crystals helium atoms dissolve only in vacancies, surrounded by Ce ions, without Gd ions in the nearest neighborhood, was discussed. MD simulations show that only this type of vacancies demonstrate an increase in concentration with increasing temperature, as well as absolute

vacancy concentration values comparable with the concentrations of dissolved helium on the “plateau” from the helium defectoscopy experimental data.

4) It is shown that the low-temperature bend on conductivity and helium solubility experimental curves is not related to the dissociation of simple complexes "impurity ion-vacancy." The discussed MD simulation results with simple dopant distributions do not demonstrate the bend on the calculated conductivity curves. Probably, in real crystals there are a large amount of regions with high local dopant concentration and the bend on experimental curves is concerned to the interaction of vacancies with these regions. Such more complex dopant distributions require further investigation.

References

[1] Haixuan Xu, Rakesh K. Behera, Yanli Wang, Fereshteh Ebrahimi, Susan B. Sinnott, Eric D. Wachsman, Simon R. Phillpot. Solid State Ionics 181 (2010) 551-556.

[2] Aaron Oaks, Di Yun, Bei Ye, Wei-Ying Chen, James F. Stubbins. J. Nucl. Mater. 414 (2011) 145-149.

[3] A. Gotte, D. Spångberg, K. Hermansson, M. Baudin. Solid State Ionics 178 (2007) 1421-1427.

[4] Hideaki Inaba, Rie Sagawa, Hideko Hayashi, Katsuyuki Kawamura. Solid State Ionics 122 (1999) 95-103.

[5] M.A. Kovalenko, A.Ya. Kupryazhkin. J. Nucl. Mater. 430 (2012) 12-19.

[6] http://code.google.com/p/idgpu/downloads/list 15.01.2013.

[7] K. Govers, S. Lemehov, M. Hou, M. Verwerft. J. Nucl. Mater. 366 (2007) 161-177.

[8] K. Govers, S. Lemehov, M. Hou, M. Verwerft. J. Nucl. Mater. 376 (2008) 66-77.

[9] S.I. Potashnikov, A.S. Boyarchenkov, K.A. Nekrasov, A.Ya. Kupryazhkin. J. Nucl. Mater. 419 (2011) 217-225.

[10] R.W. Hockney, J.W. Eastwood. Computer simulation using particles, McGraw-Hill Inc (1981).

[11] Hiroshi Deguchi, Hiroyuki Yoshida, Toru Inagaki, Masaki Horiuchi. Solid State Ionics 176 (2005) 1817-1825.

[12] Toshiyuki Mori, John Drennan, Jong-Heun Lee, Ji-Guang Li, Takayasu Ikegami. Solid State Ionics 154-155 (2002) 461-466.

[13] Hideko Hayashi, Rie Sagawa, Hideaki Inaba, Katsuyuki Kawamura. Solid State Ionics 131 (2000) 281-290.

[14] P.S. Manning, J.D. Sirman, J.A. Kilner. Solid State Ionics 93 (1997) 125-132.

[15] Hugo J. Avila-Paredes, Kwanghoon Choi, Chien-Ting Chen, Sangtae Kim. J. Mater. Chem. 19 (2009) 4837-4842.

[16] Mogens Mogensen, Thomas Lindegaard, Uffe Rud Hansen. J. Electrochem. Soc. 141 (1994) 2122-2128.

[17] G.M. Christie, F.P.F. van Berkel. Solid State Ionics 83 (1996) 17-27.

[18] T.S. Zhang, J.Ma, L.B. Kong, S.H. Chan, J.A. Kilner. Solid State Ionics 170 (2004) 209-217.

[19] T.S. Zhang, J.Ma, L.B. Kong, S.H. Chan, J.A. Kilner. Solid State Ionics 167 (2004) 203-207.

[20] V.V. Ivanov et al. Russian Journal of Electrochemistry 41 (2005) 612-619. DOI: 10.1007/s11175-005-0113-0

[21] V.N. Chebotin. Physical chemistry of solid. Chemistry, Moscow (1982).

[22] M.A. Kovalenko, A.Ya. Kupryazhkin, V.V. Ivanov. Technical Physics 55 (2010) 137-140.

[23] A.Ya. Kupryazhkin, A.Yu. Kurkin. Phys. Solid State 35 (1993) 1475.

[24] A.N. Zhiganov, A.Ya. Kupryazhkin. Technical Physics 50 (Issue 8) (2005) 1026-1033.

[25] A.Ya. Kupryazhkin, M.A. Kovalenko, A.V. Koromyslov, A.N. Zhiganov. Phys. Solid State 53 (2011) 1198-1201.

[26] D.L. Kirk, B.L. Pratt. Proc. Br. Ceram. Soc. 9 (1967) 215.

[27] P.W.M. Jacobs, S.H. Ong. J. Phys. Colloques 37 (1976) C7-331-C7-336. DOI: 10.1051/jphyscol:1976777

[28] Zhiwei Cui, Yi Sun, Yunjun Chen, Jianmin Qu. Solid State Ionics 187 (2011) 8–18.

[29] P.J. Scanlon, R.A.M. Bink, F.P.F. van Berkel, G.M. Christie, L.J. van IJzendoorn, H.H. Brongersma, R.G. van Welzenis. Solid State Ionics 112 (1998) 123–130.